

Linearized Pair-Density Functional Theory for Vertical Excitation Energies

Matthew R. Hennefarth, Daniel S. King, and Laura Gagliardi

Cite This: *J. Chem. Theory Comput.* 2023, 19, 7983–7988

Read Online

ACCESS |

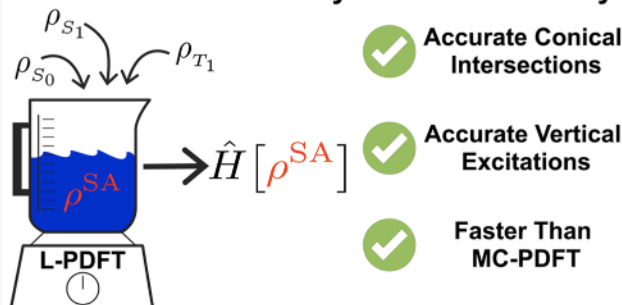
Metrics & More

Article Recommendations

Supporting Information

ABSTRACT: Multiconfiguration pair-density functional theory (MC-PDFT) is a computationally efficient method that computes the energies of electronic states in a state specific or state average framework via an on-top functional. However, MC-PDFT does not include state interaction among these states since the final energies do not come from the diagonalization of an effective model-space Hamiltonian. Recently, multistate extensions such as linearized PDFT (L-PDFT) have been developed to accurately model the potentials near conical intersections and avoided crossings. However, there has not been any systematic study evaluating their performance for predicting vertical excitations at the equilibrium geometry of a molecule, when the excited states are generally well separated. In this paper, we report the performance of L-PDFT on the extensive QUESTDB data set of vertical excitations using a database of automatically selected active spaces. We show that L-PDFT performs well on all these excitations and successfully reproduces the performance of MC-PDFT. These results further demonstrate the potential of L-PDFT, as its scaling is constant with the number of states included in the state-average manifold, whereas MC-PDFT scales linearly in this regard.

Linearized Pair-Density Functional Theory



It has been a long-standing goal of the theoretical chemical community to be able to accurately predict vertical electronic excitations, which have applications to a variety of photochemical and biochemical problems.^{1–21} Multiconfiguration pair-density functional theory (MC-PDFT)²² is a multireference electron correlation method which, starting from a qualitatively accurate multiconfigurational wave function (such as a state-average complete active space SCF (SA-CASSCF) wave function), computes a corrected energy through a nonvariational energy expression which is a functional of the electron density (ρ) and on-top pair density (Π). However, MC-PDFT is a single-state method since the final energies do not come from the diagonalization of a model-space Hamiltonian, but rather from a nonlinear functional of ρ and Π . This has been shown to lead to potential energy curves unphysically crossing near conical intersections and locally avoided crossings.^{23–26} Both conical intersections and locally avoided crossings are frequently encountered when modeling photochemistry and photodynamics, and they are characterized by regions of strong interactions between states of the same spin symmetry. To properly model these regions of nuclear configuration, it is necessary to use an electronic structure method that includes state interaction so that one obtains accurate potential energy surface (PES) topologies. In order to properly account for state interaction within the MC-PDFT framework, linearized PDFT (L-PDFT) was developed whereby the Hamiltonian is

expressed, in second quantization, as an operator that is a functional of the one- and two-particle reduced density matrices (RDMs).²⁶ The L-PDFT Hamiltonian is generated by Taylor expanding the MC-PDFT energy expression to first order in density variables about their state-average quantities within a predefined model space. L-PDFT was shown to produce similar PES topologies to XMS-CASPT2 for a variety of systems, including the spiro cation.²⁶

While L-PDFT and other MS-PDFT methods are constructed to perform well near conical intersections and locally avoided crossings, it is important that they also perform well when states are well separated. Additionally, L-PDFT has only been tested on singlet–singlet vertical excitations.²⁶ In general, we hope to have a unified PDFT method that can be broadly applied to any system and any nuclear configuration, with or without close-lying states. Furthermore, as L-PDFT models state interaction via a state-averaged modification of the electronic Hamiltonian, the energies of L-PDFT differ from those of MC-PDFT even in the absence of state interaction.

Received: August 6, 2023
Revised: September 27, 2023
Accepted: October 18, 2023
Published: October 25, 2023



Thus, it is important to demonstrate that L-PDFT performs as well as MC-PDFT in computing energy differences in even well-separated states.

Recent development of automated active-space selection schemes has made it possible to perform large-scale benchmarking of multireference methods. Recently, we have published a large-scale benchmarking of MC-PDFT and n -electron valence perturbation theory (NEVPT2)²⁷ on the QUESTDB data set^{28–33} which has over 400 vertical excitations from small-to-medium sized main group molecules. This benchmark showed that MC-PDFT performs similarly to NEVPT2, despite being significantly cheaper and less sensitive to basis set size.³⁴ All of these excitations are far enough from conical intersections/avoided crossings and represent an ideal data set to assess how L-PDFT performs in predicting vertical excitations when the states are well-separated and state-interaction effects are negligible. As the converged wave functions are freely available in a Zenodo database,³⁵ and since all MS-PDFT methods do not require any orbital reoptimization, it is computationally efficient for us to benchmark L-PDFT and other MS-PDFT methods on this data set.

We briefly review MC-PDFT²² as well as L-PDFT²⁶ (more detailed reviews can be found in their respective references) and then discuss how we can compute vertical excitations between states of different symmetries with L-PDFT. Throughout, repeated indices are summed implicitly. The MC-PDFT energy expression is given by

$$\text{PDFT} = h_p^q \gamma_q^p - \frac{1}{2} g_{pr}^{qs} \gamma_q^p \gamma_s^r - V_{\text{nuc}} - \text{ot}[\rho, \Pi] \quad (1)$$

where h_p^q and g_{pr}^{qs} are the one- and two-electron integrals, γ_q^p are elements of the 1-RDM, V_{nuc} is the nuclear–nuclear repulsion energy, E_{ot} is an on-top functional of the density (ρ) and on-top pair density (Π), and p, q, r, s are general spatial molecular orbital indices.

L-PDFT introduces state interaction by mapping a set of densities to a particular Hamiltonian-like operator, $\hat{H}^{\text{L-PDFT}}$, and then diagonalizes the model-space representation of $\hat{H}^{\text{L-PDFT}}$. $\hat{H}^{\text{L-PDFT}}$ is generated by Taylor expanding the MC-PDFT energy expression (eq 1) to first order in the 1- and 2-RDM elements (γ_q^p and γ_s^r) around some zero-order densities ($\check{\gamma}_q^p$ and $\check{\gamma}_s^r$) and extracting the effective linear operator.

$$\hat{H}^{\text{L-PDFT}} = h_p^q \mathcal{J}_p^q - V_p^q \gamma_q^p - v_{pr}^{qs} \hat{e}_{qs}^{pr} - h_{\text{const}} \quad (2)$$

$$\mathcal{J}_p^q = g_{pr}^{qs} \check{\gamma}_s^r \quad (3a)$$

$$V_p^q = \left. \frac{\partial \text{ot}}{\partial \gamma_q^p} \right|_{\check{\rho}, \check{\Pi}} \quad (3b)$$

$$v_{pr}^{qs} = \left. \frac{\partial \text{ot}}{\partial \gamma_s^r} \right|_{\check{\rho}, \check{\Pi}} \quad (3c)$$

$$h_{\text{const}} = V_{\text{nuc}} - \text{ot}[\check{\rho}, \check{\Pi}] - \left(\frac{1}{2} \mathcal{J}_p^q - V_p^q \right) \check{\gamma}_q^p - v_{pr}^{qs} \check{\gamma}_s^r \quad (3d)$$

Here, $\hat{\gamma}_q^p$ and $\hat{\gamma}_s^r$ are the 1- and the 2-electron excitation operators, respectively, \mathcal{J}^q is the Coulomb interaction with the zero-order electron density, V_p^q and v_{pr}^{qs} are the one- and two-electron on-top potentials^{36,37} evaluated at the zero-order densities, and h_{const} is a constant which only depends on the zero-order densities. The zero-order densities are taken to be the weighted average of densities within the state-average manifold.

$$\check{\gamma}_q^p = \omega_I \langle I | \hat{\gamma}_q^p | I \rangle \quad (4a)$$

$$\check{\gamma}_s^r = \omega \langle | \hat{e}_{qs}^{pr} | \rangle \quad (4b)$$

where ω_I is the same weight for state $|I\rangle$ used in the underlying SA-CASSCF or SA-CASCI calculation. Generally, we take all weights to be equal ($\omega_I = \omega_J$) such that $\check{\gamma}_q^p$ and $\check{\gamma}_s^r$ become partial traces of linear operators and therefore are independent of the basis-set representation of the model space and only dependent on the model space. In the case of a hybrid functional the final states come from a diagonalization of a weighted average of the L-PDFT Hamiltonian and electronic Hamiltonian

$$\lambda^{\text{el}} \hat{H}^{\text{el}} + (1 - \lambda) \hat{H}^{\text{L-PDFT}} \quad (5)$$

where λ controls the fraction of CASSCF to include. For the tPBE0 functional, we take $\lambda = 0.25$. The electronic Hamiltonian in second quantization is defined as

$$\hat{H}^{\text{el}} = h_p^q \hat{\gamma}_q^p - \frac{1}{2} g_{pr}^{qs} \hat{e}_{qs}^{pr} - V_{\text{nuc}} \quad (6)$$

It can be seen from eq 2 that for any model space, the L-PDFT Hamiltonian commutes with \hat{x} and \hat{z} and thus the final eigenstates will have definite spin quantum numbers. Similarly, if there is a particular spatial symmetry Ω present in the system such that $[\hat{\Omega}, \hat{H}^{\text{el}}] = 0$, then $[\hat{\Omega}, \hat{H}^{\text{L-PDFT}}] = 0$. Just like the real-electronic Hamiltonian, the L-PDFT Hamiltonian can be written as a block-diagonal matrix where only states of the same symmetry are connected (having nonzero coupling terms).

$$\begin{array}{c|ccccc} & \text{L-PDFT} & 0 & \dots & 0 \\ \text{L-PDFT} & 0 & \text{L-PDFT} & \dots & 0 \\ & \vdots & \vdots & \ddots & \vdots \\ & 0 & 0 & \dots & \text{L-PDFT} \end{array} \quad (7)$$

Here, the subscripts 1, 2, ..., n enumerate the irreducible representations. It is important to note that constructing and diagonalizing each $H_{(i)}^{\text{L-PDFT}}$ can be performed independently of one another, greatly improving the speed and memory usage over constructing and diagonalizing the entire matrix.

However, it is important to note that the zero-order densities of L-PDFT are taken to be averaged over the entire model-space, which may include averaging over states of different spatial and spin symmetries. This means that whenever there is more than one state in the state-average manifold, regardless of their symmetries, the final diagonal elements of the L-PDFT Hamiltonian will generally differ from the MC-PDFT energies. For example, if we have one singlet ($|S\rangle$) and one triplet state ($|T\rangle$), then the model space is two-

dimensional subspace defined as the span of $|S\rangle$ and $|T\rangle$. The zero-order densities for which we construct our $\hat{\gamma}_q^{L-PFT}$ in this case are taken as the average of singlet and triplet densities:

$$\hat{\gamma}_q^p = \frac{1}{2} \langle S | \hat{\gamma}_q^p | S \rangle - \langle T | \hat{\gamma}_q^p | T \rangle \quad (8a)$$

$$\hat{\gamma}_{qs}^{pr} = \frac{1}{2} \langle | \hat{\gamma}_{qs}^{pr} | \rangle - \langle T | \hat{\gamma}_{qs}^{pr} | T \rangle \quad (8b)$$

Because L-PDFT off-diagonal element coupling the singlet and triplet state are zero, $\hat{\gamma}_q^{L-PFT}$ constructed in this basis takes the form

$$\text{L-PDFT} = \begin{bmatrix} \text{L-PDFT} & S \\ S & \text{L-PDFT} \\ & T \end{bmatrix} \quad (9)$$

Again, we emphasize that $E_S^{L-PDFT} \neq E_S^{PDFT}$ since $\hat{\gamma}_q^r$ and $\hat{\gamma}_{qs}^r$ differ from the singlet 1- and 2-RDM (and similarly for the triplet state), despite the fact that H^{L-PDFT} is already diagonal.

Here, we investigate the performance of L-PDFT on the extensive data set of vertical excitations in the QUESTDB data set.^{28–33} This database includes near-FCI accuracy aug-cc-pVTZ benchmark values for a wide range of different states (valence, Rydberg, $\pi \rightarrow \pi^*$) on small-to-medium sized main-group molecules with 1–10 nonhydrogen atoms. While the ground states of these molecules are largely single reference, we have found that roughly 40% of the excited states have significant multiconfigurational character as judged by the M-diagnostic,³⁸ including a good number of double excitations.³⁴ More specifically, we use a subset of automated SA-CASSCF wave functions from our previous benchmarking^{34,35} of QUESTDB which have an unsigned tPBE0 error of less than 0.55 eV, which accounts for 439 excitations: 219 singlet, 183 triplet, and 37 doublet, including 17 double excitations. We choose this threshold to omit any possible excitations where the predominant error comes from a poor choice of the active space from the automated scheme.³⁴ We note that the nature of this threshold makes this subset of data biased in the performance of tPBE0. However, as the principal motivation of this study is to investigate whether L-PDFT can reproduce the good results of tPBE0, it is suitable for the purposes of this work.

Figure 1 summarizes the performance of SA-CASSCF, NEVPT2, tPBE, tPBE0, L-tPBE, and L-tPBE0 for this subset of data. Expectantly, we find that SA-CASSCF (mean absolute error (MUE) 0.47 eV), NEVPT2, (MUE 0.15 eV), tPBE (MUE 0.20 eV), and tPBE0 (MUE 0.15 eV) perform in correspondence with our previous benchmark values,³⁴ with a slight bias toward tPBE and tPBE0 (previous MUE of 0.24 and 0.19 eV, respectively) due to thresholding on the tPBE0 error. More importantly, one can see the close correspondence in performance between L-tPBE (MUE 0.21) and L-tPBE0 (MUE 0.16) in both the error distribution and mean absolute error on this data set of over 439 vertical excitations. Thus, we see that L-PDFT successfully reproduces the results of MC-PDFT on this extensive benchmark. Additionally, both MC-PDFT and L-PDFT agree well with the much more expensive NEVPT2 method. Furthermore, we do not see any strong relationship between the number of basis functions or number of atoms and absolute error for any of these methods (Figures S1 and S2).

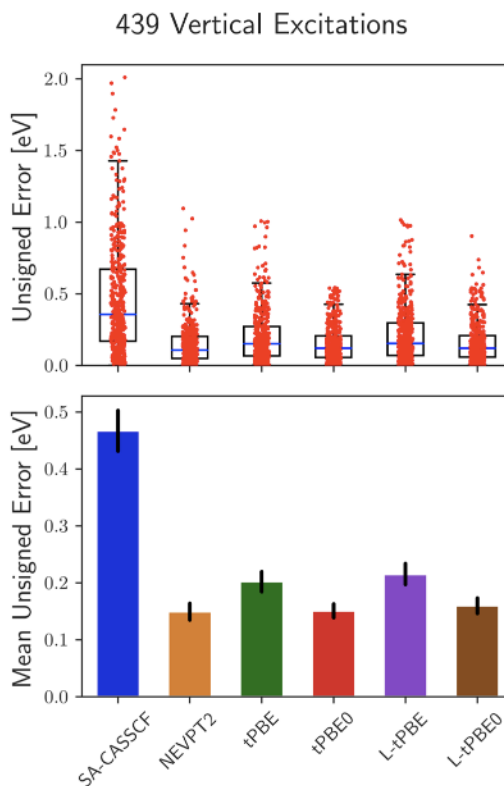


Figure 1. Distribution of the unsigned error (top) and mean unsigned error (bottom) for the vertical excitations in the whole data set for SA-CASSCF, NEVPT2, tPBE, tPBE0, L-tPBE, and L-tPBE0. The tPBE and tPBE0 labels refer to the performance of nonmultistate implementations of MC-PDFT and hybrid MC-PDFT applied to the SA-CASSCF wave functions. 95% confidence intervals for each mean are shown in black. NEVPT2 data take from ref 34.

These results are generally consistent with our prior study when we first introduced L-PDFT and showed that it performed similarly to MC-PDFT on predicting the lowest-energy spin-conserving vertical excitations for a small set of important organic chromophores.²⁶ In that small set containing 17 singlet–singlet excitations, tPBE and tPBE0 had MUE of 0.24 and 0.30 eV, respectively, whereas L-tPBE and L-tPBE0 performed slightly better with MUE of 0.20 and 0.24 eV.

Figure 2 shows how L-PDFT performs on the various types of excitations in the QUESTDB data set (singlet–singlet, singlet–triplet, valence, etc.). We see that L-PDFT performs similarly to MC-PDFT for almost all types of excitations except for the Rydberg type (Figure 2), where it performs only marginally worse (difference of several hundredths of an eV) though still much better than SA-CASSCF. In all subsets, L-tPBE0 performs similarly to the much more expensive NEVPT2 method. These results show that the state-averaged Hamiltonian of L-PDFT (eq 2) remains a robust method for calculating exciton energies on a diverse set of excited states. Even in cases where the model space is spanned by states of different spin or spatial symmetries, and hence the zero-order densities are weighted averages of densities with different symmetries (for example, singlet and triplet states), L-PDFT is able to accurately calculate excitation energies. As L-PDFT is more computationally efficient than MC-PDFT in this regard (as it requires only a single DFT quadrature calculation

Excitations By Type

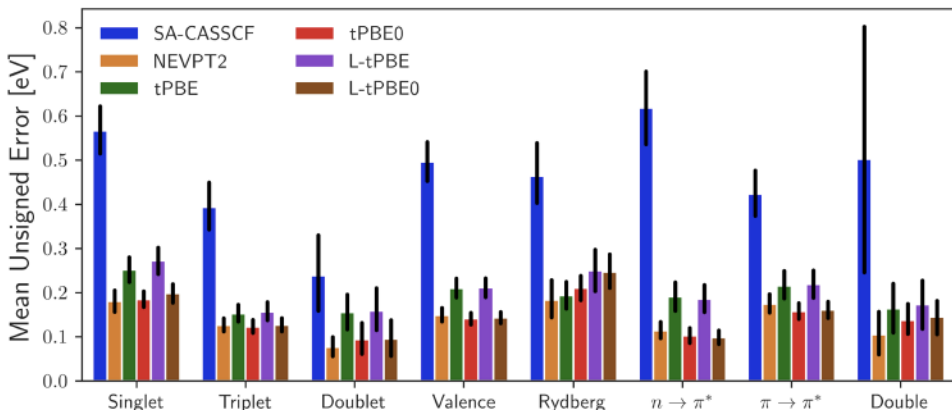


Figure 2. Mean unsigned errors of SA-CASSCF, NEVPT2, tPBE, tPBE0, L-tPBE, and L-tPBE0 by various types of excitations. The tPBE and tPBE0 labels refer to the performance of nonmultistate implementations of MC-PDFT and hybrid MC-PDFT applied to the SA-CASSCF wave functions. 95% confidence intervals for each mean are shown in black. NEVPT2 data take from ref 34.

regardless of the number of states), it appears to be a promising method for photochemical applications of MC-PDFT in general.

We also test other MS-PDFT methods, extended multistate (XMS-)²⁴ and compressed multistate (CMS-)²⁵ PDFT on a smaller multistate subset of excitations. See Section 1 of the SI for a description of these methods. We define the smaller multistate data set as those excitations where XMS- and CMS-PDFT will not necessarily reproduce the MC-PDFT vertical excitation (124 excitations) since we are only interested in the performance of MS-PDFT methods when they can differ from MC-PDFT. This set is characterized by either excitations within the same spatial and spin symmetry, or excitations to states of different spatial/spin symmetry but with at least two states in one of the symmetry manifolds.

Figure 3 summarizes the performance of XMS-, CMS-, and L-PDFT on the multistate data set as compared to MC-PDFT, CASSCF, and NEVPT2. SA-CASSCF performs the worst with a MUE of 0.58 eV and NEVPT2 performs as expected with a MUE of 0.20 eV. L-tPBE/L-tPBE0 and XMS-tPBE/XMS-tPBE0 have a mean unsigned error (MUE) of 0.28/0.20 and 0.22/0.21 eV, respectively. This is very similar to the MUE of tPBE/tPBE0 (0.24/0.18 eV). Most notably though is that CMS-PDFT performs worse than all other PDFT methods with a MUE of 0.32/0.32 eV for CMS-tPBE/CMS-tPBE0, and there are a substantial amount of excitations with an unsigned error >1.0 eV. Surprisingly, both XMS-PDFT and CMS-PDFT are less sensitive to changing the functional from tPBE to tPBE0 as compared to MC- and L-PDFT (Figure 3). Though, in the case of XMS-tPBE0, it is likely that there is little improvement to be made since the XMS-tPBE error is already close to the tPBE0 error.

Using a large database of previously converged wave functions enabled by automated active space selection,³⁴ we were able to efficiently benchmark L-PDFT on the QUESTDB data set. We find that L-PDFT performs similarly to MC-PDFT on a wide range of over 400 vertical excitations and even on excitations between states of different spatial or spin symmetry. As compared to other MS-PDFT methods, L-PDFT performs the best across a wide range of systems on computing vertical excitations (Figure 3 and Hennefarth et al.²⁶) and potential energy surfaces.²⁶ Furthermore, L-PDFT scales as a

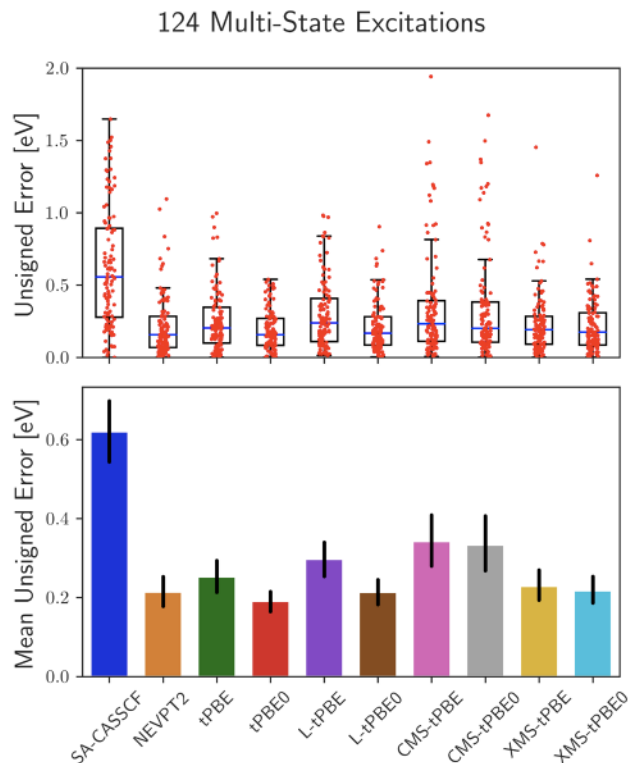


Figure 3. Distribution of the unsigned error (top) and mean unsigned error (bottom) for the vertical excitations in the multistate data set for SA-CASSCF, NEVPT2, tPBE, tPBE0, L-tPBE, L-tPBE0, CMS-tPBE, CMS-tPBE0, XMS-tPBE, and XMS-tPBE0. 95% confidence intervals for each mean are shown in black. NEVPT2 data take from ref 34.

constant with the number of states in the model space: it requires only a single DFT quadrature calculation regardless of the number of states. This makes L-PDFT an attractive method for computing vertical excitation energies in general over MC-PDFT.

In summary, we increasingly find L-PDFT to be a promising new direction within the world of PDFT, the generalization of MC-PDFT to an arbitrary number of states. It represents the best compromise between speed and accuracy, being able to

accurately predict vertical excitations when far from conical intersections, in addition to generating the correct potential energy surface topology near conical intersections and locally avoided crossings. Finally, we note the ease at which this study was performed due to the freely available converged wave functions published in the Zenodo database³⁵ and we encourage other groups to benchmark their post-SCF methods on the database as well.

■ COMPUTATIONAL METHODS

All calculations were performed in PySCF^{39,40} (version 2.2.1, tag 8eeaa7e8cab) and PySCF-forge (tag 770a04b0f1).⁴¹ Optimized SA-CASSCF orbitals from our previous benchmark study were used to calculate CASCI, XMS-PDFT, CMS-PDFT, and L-PDFT energies within these active spaces; the new SA-CASCI results were confirmed to be identical with our previously reported SA-CASSCF results. Specifically, these methods were benchmarked on the orbitals of the “Aug-(12,12)” set of active spaces, which are active spaces of size roughly (12,12) in the aug-cc-pVTZ^{42,43} basis chosen by the automated approximate pair coefficient (APC)⁴⁴ scheme; we refer the reader to our previous work for details.³⁴ All PDFT calculations utilized the default numerical quadrature grid size of 3 (50/75 radial and 302/302 angular for atoms of period 1/2 respectively) as this was found to be sufficient in our previous study.³⁴ All MS-PDFT calculations used the model space defined by the SA-CASSCF space. For L-PDFT, the zero-order densities were taken as the state-average densities within the model space.

■ ASSOCIATED CONTENT

Supporting Information

The Supporting Information is available free of charge at <https://pubs.acs.org/doi/10.1021/acs.jctc.3c00863>.

Discussion of alternative multistate PDFT methods; size-dependent analysis of CASSCF, NEVPT2, MC-PDFT, and L-PDFT; analysis of L-tPBE0 excitations which differ from tPBE0, all excitation energies (in atomic units) for each excitation and method studied (PDF)

Many .pkl files of dataframes containing the energies of each state along with the MS-PDFT intermediate state energy (HDiagPDFT) for each method and functional studied (ZIP)

■ AUTHOR INFORMATION

Corresponding Author

Laura Gagliardi – Department of Chemistry, Pritzker School of Molecular Engineering, The James Franck Institute, and Chicago Center for Theoretical Chemistry, University of Chicago, Chicago, Illinois 60637, United States; Argonne National Laboratory, Lemont, Illinois 60439, United States; orcid.org/0000-0001-5227-1396; Email: lgagliardi@uchicago.edu

Authors

Matthew R. Hennefarth – Department of Chemistry and Chicago Center for Theoretical Chemistry, University of Chicago, Chicago, Illinois 60637, United States; orcid.org/0000-0002-6601-2253

Daniel S. King – Department of Chemistry and Chicago Center for Theoretical Chemistry, University of Chicago,

Chicago, Illinois 60637, United States; orcid.org/0000-0003-0208-5274

Complete contact information is available at: <https://pubs.acs.org/10.1021/acs.jctc.3c00863>

Notes

The authors declare no competing financial interest.

■ ACKNOWLEDGMENTS

This work was supported in part by the National Science Foundation under Grant No. CHE-2054723. M.R.H. acknowledges support by the National Science Foundation Graduate Research Fellowship under Grant No. 2140001. D.S.K. was funded in part by the Eugene Olshansky Memorial Fellowship. We also acknowledge the University of Chicago’s Research Computing Center for their support of this work. Any opinion, findings, and conclusions or recommendations expressed in this material are those of the authors(s) and do not necessarily reflect the views of the National Science Foundation.

■ REFERENCES

- (1) Adamo, C.; Jacquemin, D. The Calculations of Excited-State Properties with Time-Dependent Density Functional Theory. *Chem. Soc. Rev.* 2013, 42, 845–856.
- (2) Blase, X.; Duchemin, I.; Jacquemin, D.; Loos, P.-F. The Bethe–Salpeter Equation Formalism: From Physics to Chemistry. *J. Phys. Chem. Lett.* 2020, 11, 7371–7382.
- (3) Casanova, D. Restricted Active Space Configuration Interaction Methods for Strong Correlation: Recent Developments. *WIREs Comput. Mol. Sci.* 2022, 12, No. e1561.
- (4) Dral, P. O.; Barbatti, M. Molecular Excited States through a Machine Learning Lens. *Nat. Rev. Chem.* 2021, 5, 388–405.
- (5) Eriksen, J. J. The Shape of Full Configuration Interaction to Come. *J. Phys. Chem. Lett.* 2021, 12, 418–432.
- (6) Faber, C.; Boulanger, P.; Attaccalite, C.; Duchemin, I.; Blase, X. Excited States Properties of Organic Molecules: From Density Functional Theory to the GW and Bethe–Salpeter Green’s Function Formalisms. *Philos. Trans. R. Soc. Math. Phys. Eng. Sci.* 2014, 372, 20130271.
- (7) Ghosh, S.; Verma, P.; Cramer, C. J.; Gagliardi, L.; Truhlar, D. G. Combining Wave Function Methods with Density Functional Theory for Excited States. *Chem. Rev.* 2018, 118, 7249–7292.
- (8) González, L.; Escudero, D.; Serrano-Andrés, L. Progress and Challenges in the Calculation of Electronic Excited States. *ChemPhysChem* 2012, 13, 28–51.
- (9) Izsák, R. Single-Reference Coupled Cluster Methods for Computing Excitation Energies in Large Molecules: The Efficiency and Accuracy of Approximations. *WIREs Comput. Mol. Sci.* 2020, 10, No. e1445.
- (10) Krylov, A. I. Spin-Flip Equation-of-Motion Coupled-Cluster Electronic Structure Method for a Description of Excited States, Bond Breaking, Diradicals, and Triradicals. *Acc. Chem. Res.* 2006, 39, 83–91.
- (11) Laurent, A. D.; Jacquemin, D. TD-DFT Benchmarks: A Review. *Int. J. Quantum Chem.* 2013, 113, 2019–2039.
- (12) Levine, B. G.; Esch, M. P.; Fales, B. S.; Hardwick, D. T.; Peng, W.-T.; Shu, Y. Conical Intersections at the Nanoscale: Molecular Ideas for Materials. *Annu. Rev. Phys. Chem.* 2019, 70, 21–43.
- (13) Lischka, H.; Nachtigallová, D.; Aquino, A. J. A.; Szalay, P. G.; Plasser, F.; Machado, F. B. C.; Barbatti, M. Multireference Approaches for Excited States of Molecules. *Chem. Rev.* 2018, 118, 7293–7361.
- (14) Piecuch, P.; Kowalski, K.; Pimienta, I. S. O.; McGuire, M. J. Recent Advances in Electronic Structure Theory: Method of Moments of Coupled-Cluster Equations and Renormalized Coupled-Cluster Approaches. *Int. Rev. Phys. Chem.* 2002, 21, 527–655.

(15) Roemelt, M.; Krewald, V.; Pantazis, D. A. Exchange Coupling Interactions from the Density Matrix Renormalization Group and N-Electron Valence Perturbation Theory: Application to a Biomimetic Mixed-Valence Manganese Complex. *J. Chem. Theory Comput.* 2018, 14, 166–179.

(16) Sneskov, K.; Christiansen, O. Excited State Coupled Cluster Methods. *WIREs Comput. Mol. Sci.* 2012, 2, 566–584.

(17) Westermayr, J.; Marquetand, P. Machine Learning for Electronically Excited States of Molecules. *Chem. Rev.* 2021, 121, 9873–9926.

(18) Zhou, C.; Hermes, M. R.; Wu, D.; Bao, J. J.; Pandharkar, R.; King, D. S.; Zhang, D.; Scott, T. R.; Lykhin, A. O.; Gagliardi, L.; et al. Electronic Structure of Strongly Correlated Systems: Recent Developments in Multiconfiguration Pair-Density Functional Theory and Multiconfiguration Nonclassical-Energy Functional Theory. *Chem. Sci.* 2022, 13, 7685–7706.

(19) Hedegard, E. D. In *Quantum Chemistry and Dynamics of Excited States: Methods and Applications*; González, L., Lindh, R., Eds.; Wiley, 2021; pp 47–76.

(20) Fromager, E.; Knecht, S.; Jensen, H. J. A. Multi-Configuration Time-Dependent Density-Functional Theory Based on Range Separation. *J. Chem. Phys.* 2013, 138, 084101.

(21) Hubert, M.; Hedegard, E. D.; Jensen, H. J. A. Investigation of Multiconfigurational Short-Range Density Functional Theory for Electronic Excitations in Organic Molecules. *J. Chem. Theory Comput.* 2016, 12, 2203–2213.

(22) Li Manni, G.; Carlson, R. K.; Luo, S.; Ma, D.; Olsen, J.; Truhlar, D. G.; Gagliardi, L. Multiconfiguration Pair-Density Functional Theory. *J. Chem. Theory Comput.* 2014, 10, 3669–3680.

(23) Sand, A. M.; Hoyer, C. E.; Truhlar, D. G.; Gagliardi, L. State-Interaction Pair-Density Functional Theory. *J. Chem. Phys.* 2018, 149, 024106.

(24) Bao, J. J.; Zhou, C.; Varga, Z.; Kanchanakungwankul, S.; Gagliardi, L.; Truhlar, D. G. Multi-State Pair-Density Functional Theory. *Faraday Discuss.* 2020, 224, 348–372.

(25) Bao, J. J.; Zhou, C.; Truhlar, D. G. Compressed-State Multistate Pair-Density Functional Theory. *J. Chem. Theory Comput.* 2020, 16, 7444–7452.

(26) Hennefarth, M. R.; Hermes, M. R.; Truhlar, D. G.; Gagliardi, L. Linearized Pair-Density Functional Theory. *J. Chem. Theory Comput.* 2023, 19, 3172–3183.

(27) Angeli, C.; Cimiraglia, R.; Evangelisti, S.; Leininger, T.; Malrieu, J.-P. Introduction of N-Electron Valence States for Multireference Perturbation Theory. *J. Chem. Phys.* 2001, 114, 10252–10264.

(28) Loos, P.-F.; Boggio-Pasqua, M.; Scemama, A.; Caffarel, M.; Jacquemin, D. Reference Energies for Double Excitations. *J. Chem. Theory Comput.* 2019, 15, 1939–1956.

(29) Loos, P.-F.; Scemama, A.; Blondel, A.; Garniron, Y.; Caffarel, M.; Jacquemin, D. A Mountaineering Strategy to Excited States: Highly Accurate Reference Energies and Benchmarks. *J. Chem. Theory Comput.* 2018, 14, 4360–4379.

(30) Loos, P.-F.; Scemama, A.; Boggio-Pasqua, M.; Jacquemin, D. Mountaineering Strategy to Excited States: Highly Accurate Energies and Benchmarks for Exotic Molecules and Radicals. *J. Chem. Theory Comput.* 2020, 16, 3720–3736.

(31) Loos, P.-F.; Lipparini, F.; Boggio-Pasqua, M.; Scemama, A.; Jacquemin, D. A Mountaineering Strategy to Excited States: Highly Accurate Energies and Benchmarks for Medium Sized Molecules. *J. Chem. Theory Comput.* 2020, 16, 1711–1741.

(32) Vérit, M.; Scemama, A.; Caffarel, M.; Lipparini, F.; Boggio-Pasqua, M.; Jacquemin, D.; Loos, P.-F. QUESTDB: A Database of Highly Accurate Excitation Energies for the Electronic Structure Community. *WIREs Comput. Mol. Sci.* 2021, 11, No. e1517.

(33) Loos, P.-F.; Scemama, A.; Jacquemin, D. The Quest for Highly Accurate Excitation Energies: A Computational Perspective. *J. Phys. Chem. Lett.* 2020, 11, 2374–2383.

(34) King, D. S.; Hermes, M. R.; Truhlar, D. G.; Gagliardi, L. Large-Scale Benchmarking of Multireference Vertical-Excitation Calculations via Automated Active-Space Selection. *J. Chem. Theory Comput.* 2022, 18, 6065–6076.

(35) King, D. S.; Hermes, M. R.; Truhlar, D. G.; Gagliardi, L. Large-Scale Benchmarking of Multireference Vertical-Excitation Calculations via Automated Active-Space Selection, 2022. DOI: 10.5281/zenodo.6644169.

(36) Sand, A. M.; Hoyer, C. E.; Sharkas, K.; Kidder, K. M.; Lindh, R.; Truhlar, D. G.; Gagliardi, L. Analytic Gradients for Complete Active Space Pair-Density Functional Theory. *J. Chem. Theory Comput.* 2018, 14, 126–138.

(37) Scott, T. R.; Hermes, M. R.; Sand, A. M.; Oakley, M. S.; Truhlar, D. G.; Gagliardi, L. Analytic Gradients for State-Averaged Multiconfiguration Pair-Density Functional Theory. *J. Chem. Phys.* 2020, 153, 1–12.

(38) Tishchenko, O.; Zheng, J.; Truhlar, D. G. Multireference model chemistries for thermochemical kinetics. *J. Chem. Theory Comput.* 2008, 4, 1208–1219.

(39) Sun, Q.; Berkelbach, T. C.; Blunt, N. S.; Booth, G. H.; Guo, S.; Li, Z.; Liu, J.; McClain, J. D.; Sayfutyarova, E. R.; Sharma, S.; Wouters, S.; Chan, G. K.-L. PySCF: The Python-based Simulations of Chemistry Framework. *WIREs Comput. Mol. Sci.* 2018, 8, No. e1340.

(40) Sun, Q.; Zhang, X.; Banerjee, S.; Bao, P.; Barbry, M.; Blunt, N. S.; Bogdanov, N. A.; Booth, G. H.; Chen, J.; Cui, Z.-H.; Eriksen, J. J.; Gao, Y.; Guo, S.; Hermann, J.; Hermes, M. R.; Koh, K.; Koval, P.; Lehtola, S.; Li, Z.; Liu, J.; Mardirossian, N.; McClain, J. D.; Motta, M.; Mussard, B.; Pham, H. Q.; Pulkkin, A.; Purwanto, W.; Robinson, P. J.; Ronca, E.; Sayfutyarova, E. R.; Scheurer, M.; Schurkus, H. F.; Smith, J. E. T.; Sun, C.; Sun, S.-N.; Upadhyay, S.; Wagner, L. K.; Wang, X.; White, A.; Whitfield, J. D.; Williamson, M. J.; Wouters, S.; Yang, J.; Yu, J. M.; Zhu, T.; Berkelbach, T. C.; Sharma, S.; Sokolov, A. Y.; Chan, G. K.-L. Recent Developments in the PySCF Program Package. *J. Chem. Phys.* 2020, 153, 024109.

(41) PySCF-Forge, 2022. <https://github.com/pyscf/pyscf-forge>.

(42) Dunning, T. H. Gaussian Basis Sets for Use in Correlated Molecular Calculations. I. The Atoms Boron through Neon and Hydrogen. *J. Chem. Phys.* 1989, 90, 1007–1023.

(43) Kendall, R. A.; Dunning, T. H.; Harrison, R. J. Electron Affinities of the First-row Atoms Revisited. Systematic Basis Sets and Wave Functions. *J. Chem. Phys.* 1992, 96, 6796–6806.

(44) King, D. S.; Gagliardi, L. A Ranked-Orbital Approach to Select Active Spaces for High-Throughput Multireference Computation. *J. Chem. Theory Comput.* 2021, 17, 2817–2831.